Polarized temporal impulse response for scattering media from third-order frequency correlations of speckle intensity patterns

Zhenyu Wang, Mark A. Webster, Andrew M. Weiner, and Kevin J. Webb

School of Electrical and Computer Engineering, Purdue University, 465 Northwestern Avenue, West Lafayette, Indiana 47907-2035

Received March 3, 2006; revised June 28, 2006; accepted June 28, 2006; posted July 10, 2006 (Doc. ID 68519)

Second- and third-order frequency correlations of speckle intensity patterns are used to characterize scattering media for multiple polarization states. The polarized temporal responses thus obtained are sensitive to the degree of scatter, with results being predictable by a diffusion model with sufficiently strong scatter. Experimental data are used to reconstruct various transfer functions. © 2006 Optical Society of America

OCIS codes: 030.6140, 290.4210, 290.1990, 290.7050, 100.5070.

1. INTRODUCTION

In recent years, there has been increasing interest in imaging through scattering media. The optical characterization of materials where there is significant scatter, or optical imaging within or through such highly scattering media, has applications as varied as soft tissue imaging, the study of polymer composites, and the evaluation of sea ice constituents. In particular, there has been recent activity related to biomedical optical imaging, where images based on a diffusion equation model, optical diffusion tomography (ODT), have been determined using optimization methods,[1,2] and fluorescence contrast[3,4] and targeting[5] have been utilized. The coherence of the light is also important when trying to image in scattering media using speckle techniques.[6]

Polarization information provides opportunities when the total scatter is modest.[7,8] Polarized light incident on a scattering medium becomes depolarized due to multiple scattering events, ultimately resulting in no memory of the initial state of polarization in the case of strong scatter. In this strong scatter limit, the scalar diffusion equation applies,[9,10] and this model can be used to obtain an estimate of the photon path length distribution or temporal response for the scattering medium.[11] However, in the case of lesser amounts of scatter, there will be some memory of the initial polarization of the incident light. In this regime, multiple polarization state measurements can provide additional information about the medium. Hence, use of multiple incident and detected polarization configurations may provide data which could allow enhanced imaging of scattering media and information on the scatterers. There have been a number of studies of polarization memory with multiply scattered light.[12–17] Imaging based on polarization information,[18] such as polarization-difference imaging,[19] has been suggested. Improvement of image resolution through the use of polarized light, where the more weakly scattered photons are selected, has been proposed.[20] Also, there have been empirical studies of the relationship between depolarization and particle size or concentration,[12,21,22] which have used depolarization parameter[14] and depolarization length[12] descriptions.

The study of the field and intensity statistics and their various correlations is fundamental to the description of scattering media. The statistical properties of the speckle intensity contains information about the optical properties of the scattering medium and the coherence of the source.[6] The second-order speckle intensity correlation has proven to be a powerful tool. For example, Genack used the autocorrelation of the intensity fluctuation, as the laser frequency was tuned, in the study of disordered media.[23] Third-order correlations and bispectral techniques have also been used to retrieve information from scattering media. For example, Shirley and Lo used this technique in remote sensing of a scattering object's size, shape, and surface property.[24] Webster *et al.* also discovered that the use of third-order correlations of speckle intensity patterns in frequency, in conjunction with bispectral techniques, allows for the reconstruction of the temporal response of a scattering medium.[25]

Recently, the statistics of the scattered field were directly measured using an interferometer setup, and the zero-mean complex Gaussian statistics for the polarized field from weakly scattering media were verified.[26,27] This result indicates that the work of Webster *et al.*[25] can be extended to multiple polarization states and to studies of materials in a sufficiently weakly scattering regime such that polarization information becomes important. Here we describe the polarization-dependent results of the second- and third-order speckle intensity correlations of measured data for samples having relatively weak scatter.

2. THEORY

A. Scattered Field

When coherent light is scattered from a rough surface or the volume of a scattering medium, the total field at a

particular point in space with particular polarization can be viewed as the superposition of many scattered partial waves, each of which has a random magnitude and a random phase. This allows for the total field $E_o(\nu)$ to be expressed as a random phasor sum by[28]

$$E_o(\nu) = \frac{1}{\sqrt{N}} \sum_{k=1}^{N} A_k \exp[-j\phi_k(\nu)], \tag{1}$$

where A_k is the random magnitude, and $\phi_k(\nu)$ is the random phase of the kth elementary partial wave. The number of elementary partial waves is given by N, which is assumed to be large such that the limit of $N \to \infty$ can be used. The model is valid when the so-called weakly scattering assumption is satisfied, which requires that the mean free path length (average distance between two successive scattering events) is much larger than the wavelength of the light in the medium. Under this assumption, the output field $E_o(\nu)$, measured at a single frequency ν and modeled by the random phasor sum in Eq. (1), has first-order statistics that are zero-mean circular complex Gaussian. Because of this, the Gaussian moment theorem of Reed can be used to express high-order moments as a product of second-order moments.[29]

Consider the vector electric field in Cartesian form, with a linearly polarized (LP) basis set, as

$$\mathbf{E}(\nu) = [\hat{\mathbf{x}}E_x(\nu) + \hat{\mathbf{y}}E_y(\nu)]\exp(-jkz) + \text{c.c.}, \tag{2}$$

where propagation in the z direction is implied, and $\hat{\mathbf{x}}$ and $\hat{\mathbf{y}}$ are unit vectors. Alternatively, a circular polarized (CP) basis can be used, giving

$$\mathbf{E}(\nu) = [\hat{\mathbf{R}}E_R(\nu) + \hat{\mathbf{L}}E_L(\nu)]\exp(-jkz) + \text{c.c.}, \tag{3}$$

where $\hat{\mathbf{L}}$ and $\hat{\mathbf{R}}$ are unit vectors for right-hand and left-hand circular polarization (RHCP, LHCP), respectively. In the presence of scattering centers, the scattered field usually has both components even if the input contains only one polarization. This can be shown in the simple case of light scattering by a homogeneous dielectric sphere.

Considering scattering from a single scatterer presents insight into the multiple-scatter regime using a simple model. Figure 1 shows the geometry for scattering from a homogeneous sphere with the incident field x polarized and incident along the z direction ($\theta=0$). The scattered wave E_o at a certain scattering angle θ is shown. The solution to this type of scattering problem was formulated by Mie.[30] Figure 2 shows an example calculation from the Mie field expansion assuming that the incident wave is linearly polarized in the x direction, as in Fig. 1, an incident wave of wavelength 850 nm and a single spherical TiO_2 particle of 50 nm diameter. A refractive index of 2.70 was used for TiO_2, and the background was assumed to have a refractive index of 1.49. As the size of the scattering sphere is much smaller than the wavelength of the incident wave, the problem has the features of Rayleigh scatter. The upper half of Fig. 2 gives the ϕ-integrated (the angle measured from x toward y in Fig. 1) power density as a function of scattering angle θ for the three linearly polarized scattered field components. The scattered intensities are normalized to the maximum of the x component at $\theta=0$, and the y and z components are scaled up by a factor of 3 for clarity. The x component or copolarized scattered light is dominant and contains most of the energy. The result in the lower half of Fig. 2 shows the case for incident RHCP light, and the scattered RHCP and LHCP light has been plotted as intensity angular distributions. For RHCP incident light, roughly half the scattered energy is backscattered into LHCP light and half is forward scattered as RHCP light, i.e., approximately 50% of the scattered power is in copolarized light. In contrast, with LP input light, approximately 80% of the scattered power is retained as copolarized light. This result suggests that for a single spherical scatterer, LP light retains its initial polarization state (in copolarization) better than CP light. In both cases, the scattered light in the forward direction is highly copolarized and has the same intensity at $\theta=0$. From Fig. 2, for LP incident light, 40% of the total

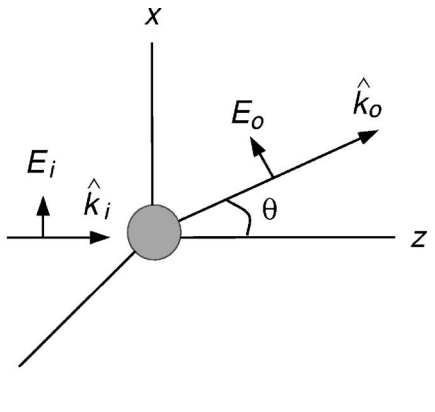

Fig. 1. Incident field E_i propagating along the z axis is scattered by a homogeneous sphere at the origin, and the scattered field E_o with a scattering angle θ is shown.

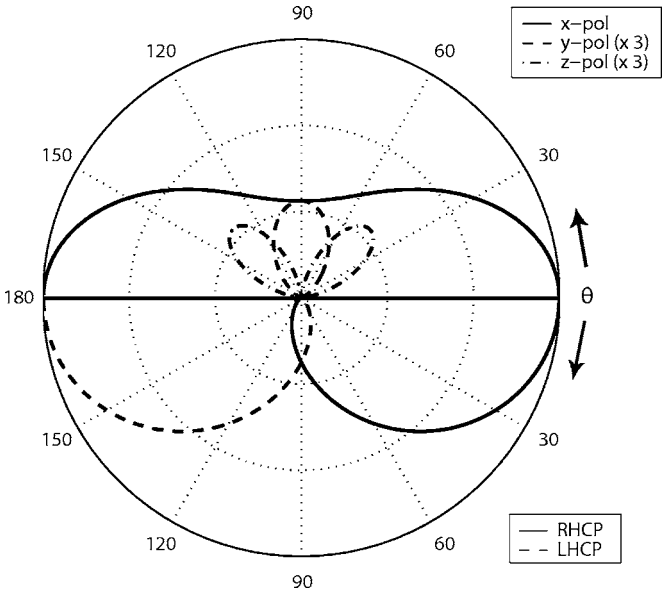

Fig. 2. Intensity angular distribution for light scattered from a small sphere. In the upper half, the incident field is x-polarized (LP), incident in the z direction ($\theta=0$), and the x-, y-, and z-polarized components of the ϕ-integrated scattered light intensity are plotted. The y and z components have a magnification of 3. In the lower half, the incident wave is z-directed RHCP, and RHCP and LHCP components for the scattered light intensity angular distribution are plotted.

scattered light is scattered as copolarized light in the forward direction ($\theta \in [0, \pi/2]$), while 5.0% is forward scattered as y-polarized light, measured as cross-polarized light. For CP, 43.7% of the total scattered light is forward scattered as copolarized light and 6.3% as cross-polarized light.

For our interest of multiple scattering, the scattered field is the ensemble of light with different trajectories undergoing a series of scattering events. As light propagates through the scattering medium, memory of the initial polarization information is gradually lost, i.e., depolarization occurs. As Fig. 2 shows that more cross-polarized light is generated per scattering event for a CP input, we may anticipate that CP light will depolarize more quickly (with scatter or sample thickness) than the case of linearly polarized incident light. With a transmission measurement and a given amount of scatter, the fact that Fig. 2 shows that more cross-polarized light for CP input light is forward scattered indicates that the temporal response for multiple scatter may be more peaked at early times, relative to the LP case. Our measured data will prove to support these speculations. Furthermore, with weak scatter, one can expect that polarization data can provide information on the scatterers themselves.

B. Light Propagation in Scattering Media

Polarized light propagating in a medium with appropriate scatter can be described by the radiative transfer equation (RTE) (see Chandrasekhar[31]), which is a model based on the particle nature of light and thereby governed by conservation of momentum, i.e., in its scalar form it is the Boltzmann transport equation.[32] There are many situations, notably in the regime where polarization information could be valuable, where the diffusion equation is inadequate and where it is still impractical to solve Maxwell's equations. The transport equation may be of importance in this regime. Typical solutions to the scalar form of the transport equation use Monte Carlo techniques with some simple model for the scattering,[33–35] and a few have studied the more complex vector solution.[8,17,36]

In many cases involving stronger scatter, solving the transport equation directly is not necessary, and the P_1 approximation to the RTE, from a Legendre series expansion,[32] i.e., the diffusion equation, can be used. In terms of the radiative flux density, $\Phi(\mathbf{r},t)$ (in units of W m^{-2}), the diffusion equation is

$$\frac{\partial}{\partial t}\Phi(\mathbf{r},t) + v\mu_a\Phi(\mathbf{r},t) - \nabla\cdot[D\nabla\Phi(\mathbf{r},t)] = vS_0(\mathbf{r},t), \quad (4)$$

where v is the transport velocity, $D = v/3(\mu_s' + \mu_a)$ is the diffusion coefficient (in units of m^2 s^{-1}), μ_s' (m^{-1}) is the reduced scattering coefficient, μ_a (m^{-1}) is the absorption coefficient, and $S_0(\mathbf{r},t)$ is the source. The diffusion approximation does not hold near boundaries or sources or in strongly absorbing media, but is valid for a wide range of random media of interest. In practice, sample thicknesses more than an order of magnitude greater than the transport mean free path $l^* = 3D/v$ are needed for the diffusion approximation to be valid in a transmission geometry. For the scattering samples we used, $\mu_a \ll \mu_s'$, so $\mu_a = 0$ is assumed. The Green's function for Eq. (4) with, for example, a scattering slab of finite thickness, can be found from image theory, assuming an interface with free space, which can be represented as $\Phi = 0$ on an extrapolated boundary.[37]

The intensity temporal response of a random medium is very important for characterization of the optical properties. It is equal to the time-of-flight distribution function for the scattered light when pulsed input light is used and, assuming it applies, can be obtained from the Green's function for the diffusion equation. We use a Dirac delta function source term, $S_0(\mathbf{r},t) = \delta(\mathbf{r}',t)$, where $\mathbf{r}'$ is the source location, to solve Eq. (4), and to obtain an expression for the radiative flux density at a particular observation point. From Fick's law,[32] the radiative current density $\mathbf{J}(\mathbf{r},t)$ (in units of W m^{-2}), describing power flow, can be found under the diffusion approximation, resulting in

$$\mathbf{J}(\mathbf{r},t) = -\frac{D}{v}\nabla\Phi(\mathbf{r},t). \quad (5)$$

The intensity at the observation point measured by a photodetector is $I_D(t) = \hat{\mathbf{n}}\cdot\mathbf{J}$, where $\hat{\mathbf{n}}$ is the detector normal unit vector. Normalizing this result gives the time of flight distribution as

$$p_D(t) = \frac{I_D(t)}{\int_{-\infty}^{\infty} \mathrm{d}t\, I_D(t)}. \quad (6)$$

Equation (6) can be interpreted as the ensemble average temporal impulse response for regimes where the diffusion model applies.[25]

C. Polarized Intensity Temporal Response

The polarization of light can be fully described by the four elements of the Stokes vector, the measurement of which is possible through standard procedures.[38] Assuming propagating in the z direction, light of the arbitrary polarization state may be represented by a Stokes vector of the form[38]

$$S = \begin{pmatrix} I \\ Q \\ U \\ V \end{pmatrix} = \begin{pmatrix} E_x E_x^* + E_y E_y^* \\ E_x E_x^* - E_y E_y^* \\ E_x E_y^* + E_y E_x^* \\ j(E_x E_y^* - E_y E_x^*) \end{pmatrix}, \quad (7)$$

where I represents the total light intensity, Q and U represent the LP components of the beam, V represents the CP components, and the asterisk indicates complex conjugate. With this notation, the linear x- and y-polarized intensities are given by $(I+Q)/2$ and $(I-Q)/2$, respectively, while the LHCP and RHCP intensities are given by $(I+V)/2$ and $(I-V)/2$, respectively.

One can define a normalized ensemble average intensity temporal response for a given input and output polarization state, and based on Eq. (6), this is

$$p_{ij}(t) = \frac{\langle I_{ij}(t)\rangle}{\int_{-\infty}^{\infty} \mathrm{d}t \langle I_{ij}(t)\rangle}, \tag{8}$$

where the subscripts i and j designate the input and output polarizations, respectively: x and y for linear polarization, l for LHCP, and r for RHCP. The quantities $p_{ij}(t)$ are measurable and can be obtained from the Stokes vector formalization of Eq. (7).

D. Speckle Intensity Correlations

Genack and Drake[39] give the second-order correlation between two fields at different frequencies as

$$\langle E(\nu + \Delta\nu)E^*(\nu)\rangle = \langle I\rangle P(\Delta\nu), \tag{9}$$

where $P(\Delta\nu)$ is the Fourier transform of the temporal response $p(t)$ for a particular polarization, given by

$$P(\Delta\nu) = \int_{-\infty}^{\infty} \mathrm{d}t\, p(t)\exp(-j2\pi\Delta\nu t). \tag{10}$$

We drop the polarization subscripts i and j for simplicity, with the assumption that they are implied. The measured data we show was obtained for various input–output polarization states. From the uncertainty relation, $E(\nu)$ becomes uncorrelated with $E(\nu+\Delta\nu)$ when the shift in frequency $\Delta\nu$ satisfies the condition of $\Delta\nu\Delta t \sim 1$, where Δt is a measure of the width of $p(t)$, which can be seen from the Fourier transform relation in Eq. (10).

In practice, it is usually difficult to measure the field statistics of Eq. (9) directly at optical frequencies for scattered light. Instead, it is more practical to measure the second-order intensity correlation $\langle I(\nu+\Delta\nu)I(\nu)\rangle$. This correlation is fourth order in the electric field, and since the field has circular complex Gaussian statistics, the Gaussian moment theorem[29] can be applied along with Eq. (9) to give[25]

$$\langle \tilde{I}(\nu + \Delta\nu)\tilde{I}(\nu)\rangle = |P(\Delta\nu)|^2, \tag{11}$$

where $\tilde{I} = (I - \langle I\rangle)/\langle I\rangle$ is a normalized intensity for mathematical convenience.

The second-order intensity correlation contains information about the Fourier magnitude of $p(t)$, but not the Fourier phase, as seen from Eq. (11). It is therefore not possible to reconstruct the temporal response $p(t)$ from the sole measurement of second-order intensity correlations without using *a priori* information.

It was recently discovered[25,40] that third-order intensity correlations do contain sufficient information about the Fourier phase of $p(t)$, allowing for the reconstruction of $p(t)$ from intensity-based measurements without any assumed model for $p(t)$. The third-order intensity correlation, which is a sixth-order field correlation, can again be evaluated by the Gaussian moment theorem[29] with the use of Eq. (9) to give[25,40]

$$\langle \tilde{I}(\nu)\tilde{I}(\nu + \Delta\nu_1)\tilde{I}(\nu + \Delta\nu_1 + \Delta\nu_2)\rangle = 2\,\mathrm{Re}\{P(\Delta\nu_1)P(\Delta\nu_2)P^*(\Delta\nu_1 + \Delta\nu_2)\}. \tag{12}$$

Therefore, the third-order correlation is equal to twice the real part of the bispectrum of the temporal response function $p(t)$.[25,40] Bispectral techniques have been used in other applications.[41,42] The result in Eq. (12) allows for the Fourier phase to be reconstructed from the bispectral phase through the relation

$$\psi(\nu_1, \nu_2) = \phi(\nu_1) + \phi(\nu_2) - \phi(\nu_1 + \nu_2), \tag{13}$$

where $\phi(\nu_1)$ and $\phi(\nu_2)$ are the Fourier phase at optical frequency ν_1 and ν_2, respectively, and $\psi(\nu_1, \nu_2)$ is the bispectral phase obtained from third-order intensity correlation, as in Eq. (12).

We obtained $|P(\Delta\nu)|$ from Eq. (11) and the Fourier phase from Eq. (12) using an explicit iterative scheme,[25,40] thereby producing $p(t)$ with an arbitrary time offset (i.e., the third-order correlation is insensitive to time offset) using an inverse Fourier transform. This is the procedure we used for speckle intensity measurements with various incident and detected polarization states [giving $p_{ij}(t)$]. After retrieving the Fourier magnitude and Fourier phase from intensity correlations, we applied a Hamming window[43] to determine the temporal responses from measured data, giving $p_H(t) = p(t) * w_H(t)$, where $p_H(t)$ is the windowed result, $p(t)$ is the retrieved temporal response without the Hamming window. $w_H(t)$ is the window function,[43] and $*$ is the convolution operator. This procedure is to prevent ripple artifacts due to the finite measurement bandwidth. For the case of a Hamming window applied to the data measured with a 80 GHz bandwidth, the temporal resolution was approximately 12 ps, adequate for the scattering samples we used. In the remainder of the paper, we do not differentiate between $p(t)$ and $p_H(t)$.

3. EXPERIMENT

The experimental setup used to study the polarization behavior of speckle patterns and the ensemble averaged temporal impulse response is shown in Fig. 3. The tunable laser source used was an external cavity (Littman–Metcalf design) laser diode (New Focus Vortex 6017), which provided frequency scanning up to approximately 80 GHz. It has a single-mode output with a narrow linewidth of approximately 5 MHz, which gives a coherence length of approximately 60 m, much greater than the average path lengths (of the order of centimeters) for photons propagating in the scattering media we studied. Suitably high coherence is required to achieve Gaussian field statistics (and negative exponential intensity statistics).[28] The light source had a center wavelength at approximately 850 nm and an average power of 10 mW. An optical isolator was used to prevent back reflections, which may destabilize the laser output. A small portion of the output power was coupled into a scanning Fabry–Perot interferometer, using the half-wave plate (HWP) retarder and polarization beam splitter (PBS) combination, to monitor the laser diode center frequency, and most of the output power was focused onto the front face of the scattering random medium by the lens L1.

The scattering samples used in the experiment were commercial white acrylics (Cyro Industries, Acrylite FF) with the scatterers composed of small TiO_2 particles of average diameter approximately 50 nm. The reduced

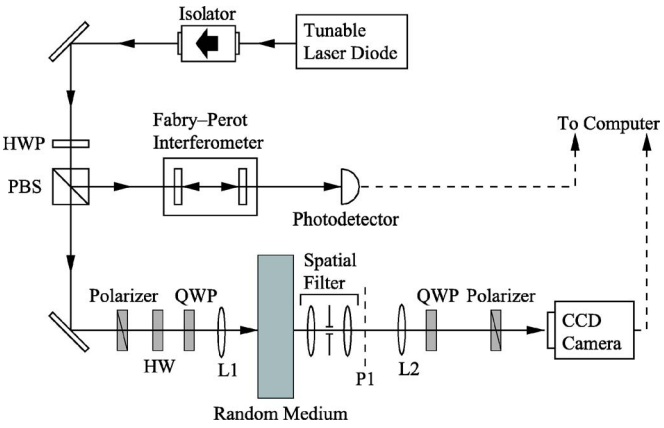

Fig. 3. (Color online) Experimental setup used to measure the speckle intensity patterns as a function of the laser diode center frequency. The Fabry–Perot interferometer is used to monitor the change in the laser diode center frequency as it is tuned. Lens L1 ($f_{L1}=50$ mm) focuses the laser output onto the front face of the scattering random medium. The spatial structure of the speckle pattern at plane P1 is controlled by the unity magnification spatial filter. Lens L2 ($f_{L2}=75$ mm) provides a magnification factor of $M=10$ from the plane P1 to the CCD image plane, where the resultant frequency-dependent speckle pattern is obtained. The combination of polarizer, half-wave plate (HWP) and quarter-wave plate (QWP) before lens L1 is used to control the polarization of the input beam and the polarizer plus QWP after L2 is to select the desired output polarization.

scattering coefficient in a diffusion model was $\mu_s'=4\ \mathrm{cm}^{-1}$, corresponding to a transport mean free path of 0.25 cm, the mean distance for the photon direction to be randomized.[32]

A small area from the back of the scattering medium (approximately $0.90\ \mathrm{mm}\times 0.67\ \mathrm{mm}$) was imaged onto a cooled CCD camera (CoolSNAP HQ from Roper Scientific, Inc.) with 1392×1040 pixels of size $6.45\ \mu\mathrm{m}\times 6.45\ \mu\mathrm{m}$. The input beam and the detection spot were colinear. Hence, the CCD camera captured the forward-scattered light and quasi-ballistic light. The imaging optics consisted of a spatial filter in a $4f$ telescope configuration that gave unity magnification at the plane P1 and another lens L2 that provided a magnification of 10 from the plane P1 to the CCD image plane. The spatial filter was formed by two identical achromatic lenses of focal length $f=50$ mm and an adjustable iris aperture, located at the Fourier focal plane. The aperture was used to control the spatial feature size of the speckle so that the CCD camera adequately resolved each spot and so that there were adequate independent samples in the image, i.e., enough spots for good statistics. The feature size of speckle can be approximated by the Airy pattern, which gives that the central spot for light passing through a small circular aperture has a spot size radius of approximately $r=1.22\lambda z_i/D$, where λ is the wavelength, z_i is the image distance, and D is the diameter of the aperture.[44] In our experiment, we used an aperture of radius 1 mm and the resulting speckle spots had a radius of approximately 0.5 mm at the CCD camera plane.

The combination of polarizer, HWP and quarter-wave plate (QWP) was placed before the scattering sample to control the input polarization state. The output polarization was selected by placing a QWP and a polarizer before the CCD camera. The whole data acquisition process was controlled through a computer interface by a program written in LABWINDOWS. As the light frequency was scanned, a series of intensity speckle patterns were captured by the CCD camera and sent to the computer for data processing.

4. RESULTS AND DISCUSSION

A. Intensity Speckle Pattern

An example speckle pattern from the samples studied is shown in Fig. 4(a). This is a measured pattern for a case where the input and output light are both RHCP, $\mu_s'=4\ \mathrm{cm}^{-1}$, and the sample thickness is 9 mm. The intensity histogram calculated from the speckle image in Fig. 4(a) is presented as a semilogarithmic plot in Fig. 4(b). The speckle intensity statistics are therefore modeled well by a negative exponential probability density function, given by $p_I(I)=\langle I\rangle^{-1}\exp(-I/\langle I\rangle)$, where $\langle I\rangle$ is the mean intensity. This suggests that the fields are zero mean circular complex Gaussian, allowing for the intensity correlations of Subsection 2.D to be applied. Recently, Gerke *et al.*, for the first time, directly measured the polarized field statistics for weakly scattering samples, including a sample with the same scattering (a 9 mm sample with $\mu_s'=4\ \mathrm{cm}^{-1}$) and found the transmitted light to have zero mean circular Gaussian field statistics.[27] We have found that the sample thickness should be greater than the mean free path l^* to obtain a negative exponential intensity distribution. We can therefore proceed with confi-

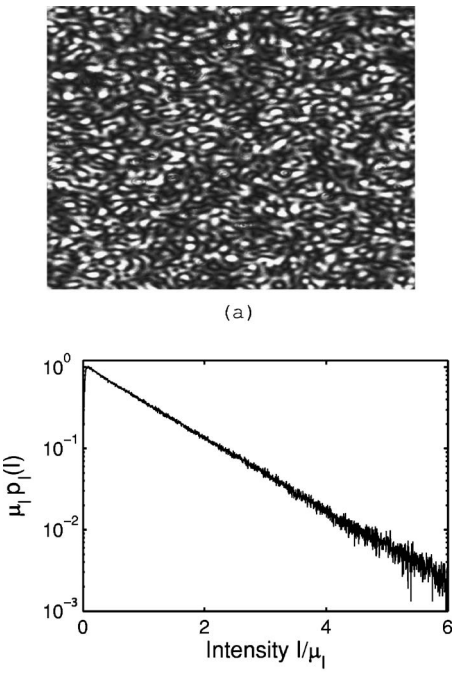

Fig. 4. (a) Typical intensity speckle pattern from the scattering media studied, captured by a CCD camera, for a 9-mm-thick sample having $\mu_s'=4\ \mathrm{cm}^{-1}$. The input and output light are both RHCP. (b) Intensity histogram obtained from the speckle pattern given in (a) plotted on a semilogarithmic scale. The negative exponential intensity probability density function fit to the result in (b) is indistinguishable.

dence in using the second- and third-order intensity correlations with frequency for the samples we present.

For even less scattering media, because of the strong ballistic light, the field statistics deviate from zero mean, resulting in the field being a constant phasor plus a random phasor sum.[45] Similar results for microwave field transmission in a random medium were also obtained by Chabanov and Genack[46] and Garcia-Martin *et al.*,[47] in both experiment and theory. Deviations from zero mean circular Gaussian field statistics for optically thin random media preclude the approach we present for the use of the intensity frequency correlations as a means to determine the ensemble average impulse response.

B. Degree of Polarization

Light loses its initial polarization state with increasing scatter, i.e., with increasing distance into the scattering medium. The samples we measured had thicknesses ranging from 3 to 21 mm. The measured mean intensity as a function of sample thickness is shown in Fig. 5, with fixed input power. Notice that while the copolarized light for both LP and CP input appear similar (on a linear scale, it becomes clear that for thin samples, the mean for the LP case is slightly higher), the cross-polarized CP mean is appreciably higher for the thinner samples. From the Mie scattering result for a single spherical scatterer, shown in Fig. 2, for CP there is more forward-scattered cross-polarized light generated per scattering event, supporting our measurement result.

We define the degree of polarization as

$$P = \frac{\langle I_{\parallel} \rangle - \langle I_{\perp} \rangle}{\langle I_{\parallel} \rangle + \langle I_{\perp} \rangle}, \tag{14}$$

where $\langle \cdot \rangle$ is a spatial ensemble average over the intensity speckle statistics for a specific polarization, $I_{\parallel}$ is the intensity in the copolarized state, i.e., the same polarization as that incident, and $I_{\perp}$ is the cross-polarized light intensity. For LP, $I_{\parallel}$ is measured as I_{xx}, and $I_{\perp}$ as I_{xy}. Because the scattering samples used were homogeneous and contained spherical scatterers, we have $I_{xx}=I_{yy}$ and $I_{xy}=I_{yx}$. Likewise for CP, $I_{\parallel}=I_{ll}=I_{rr}$ and $I_{\perp}=I_{lr}=I_{rl}$. Hence, we can obtain P for LP and CP, respectively. The measured degree of polarization as a function of thickness for the samples is shown in Fig. 6. The input light, either CP or LP, initially has $P=1$ or is perfectly polarized. With increasing scatter, the degree of polarization decreases and eventually goes to zero at a scatter level where polarization information is lost. From Fig. 6, the light is nearly completely depolarized at a thickness of 18 mm, which is approximately seven times the transport mean free path. We can consider this as the characteristic length for depolarization for the scattering materials we used. The data in Fig. 6 indicate that, indeed, LP light depolarizes more slowly that CP light. This is again consistent with the single-scatterer model of Fig. 2. In a previous work, it was also found that for small scatterers, relative to the wavelength, LP light maintains its polarization better than CP light, whereas for moderate, or large-sized scatterers (comparable to or large with respect to the wavelength), CP light was found to maintain its polarization better than LP light.[13,48] The 50 nm TiO_2 particles in the samples we tested at a wavelength of 850 nm are in the small scatterer regime.

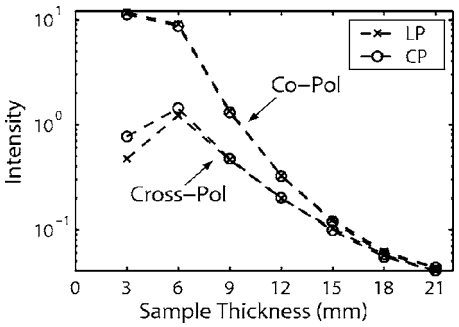

Fig. 5. Measured mean intensity for copolarized and cross-polarized light for LP and CP input as a function of sample thickness, with input power fixed. The sample has $\mu_s'=4\ \mathrm{cm}^{-1}$.

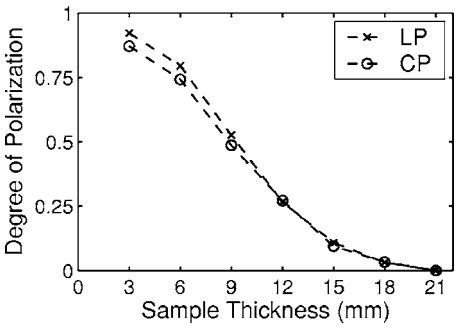

Fig. 6. Degree of polarization as a function of sample thickness: linear polarization (crosses), circular polarization (circles). The sample has $\mu_s'=4\ \mathrm{cm}^{-1}$.

C. Polarized Intensity Frequency Correlations

By scanning the frequency of the laser diode, we obtained a sequence of speckle patterns as a function of frequency and performed speckle intensity correlations. Figure 7 shows the second-order correlation (autocorrelation) function of the measured speckle patterns for various polarizations and sample thicknesses. There are significant differences between the copolarization and cross-polarization results for the thinner samples. Where there is polarization information, the copolarized light decorrelates more slowly with frequency than the cross-polarized light for both LP and CP input light, a difference that diminishes with increasing sample thickness. The spectral width of the second-order correlation is a measure of the temporal features in $p(t)$, where a more rapid temporal response results in broader spectral content. The copolarized light has significant quasi-ballistic content, and hence the response decorrelates with frequency more slowly. While the depolarization in Fig. 6 relates to the temporal integral of the unnormalized $p_{ij}(t)$, i.e., the mean intensity, the second-order correlation in Fig. 7 is a measure of the temporal variation. The copolarized results for LP and CP are virtually identical. While the scattered light from a single scatterer for the two cases has significant differences (see Fig. 2), the copolarized light features for the thinner samples in Fig. 7 are dominated by the quasi-ballistic light, which is largely forward scattered and hence effectively retains the incident polariza-

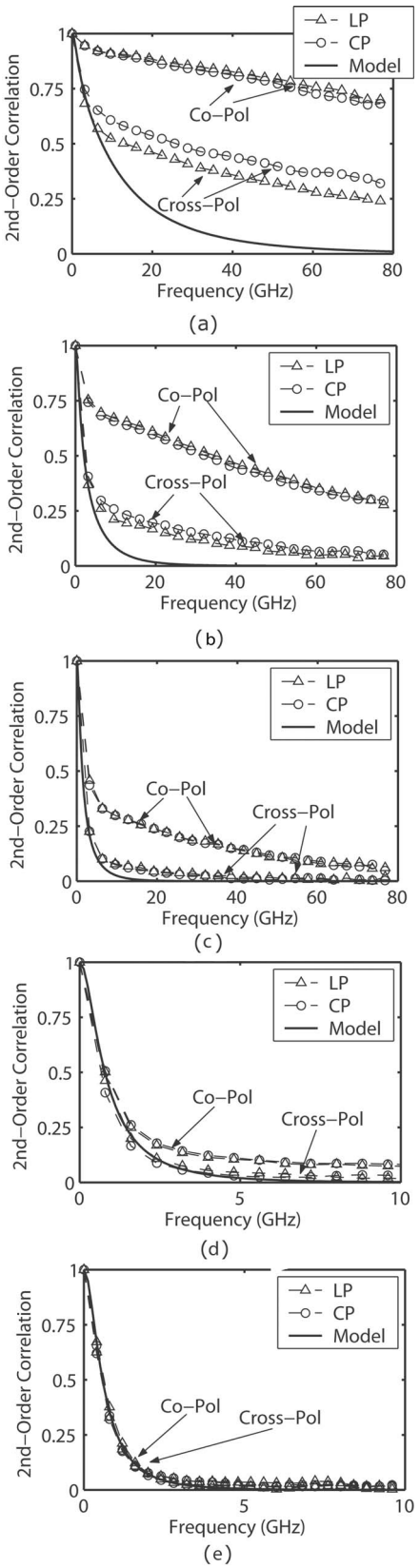

Fig. 7. Second-order intensity correlations for copolarized and cross-polarized light for scattering samples of various thickness for samples thicknesses of (a) 6 mm, (b) 9 mm, (c) 12 mm, (d) 15 mm, and (e) 18 mm. The triangles show linear polarization and the circles show circular polarization. The solid curves are calculated from a diffusion model using $\mu_s' = 4\ \mathrm{cm}^{-1}$.

tion. The copolarized light is less sensitive to the initial input polarization. For cross-polarized light, the intensity in the forward direction after a single-scattering event is very small, as shown in Fig. 2. Therefore, cross-polarized light measured in the forward direction has more multiple-scattering features and hence a more slowly varying temporal response and a more rapid decorrelation with frequency. We find it interesting that for the two thinnest samples, the CP cross-polarized light decorrelates more slowly with frequency than the LP result. From Fig. 2, more cross-polarized light is forward scattered in the CP case, which suggests a more peaked temporal response and a broader correlation bandwidth. While a model that represents the multiple scatter in this regime is necessary to completely understand the effect, it appears that the single-scatterer result is consistent with the cross-polarized intensity correlations of Fig. 7.

The results from a diffusion model for the slab problem[37] are given in Fig. 7. This model is appropriate when the light is totally randomized in direction and polarization. In our experiment, the 18-mm-thick sample appears to fall into this category, and that case, in Fig. 7(e), shows excellent agreement between the measured data and the model. This regime allows $\mu_s' = 4\ \mathrm{cm}^{-1}$ to be extracted (μ_a is assumed to be zero). For sample thicknesses less than 18 mm, the second-order correlation shows polarization dependence. In moderate scatter regimes, it appears that the cross-polarized light is better approximated by the diffusion model [see Figs. 7(c) and 7(d)], while the copolarized result deviates significantly from this model. The cross-polarized light has more multiple-scatter influence and is better represented by a diffusion process. In the thinnest samples [see Figs. 7(a) and 7(b)], both copolarization and cross-polarization results are quite different from the model, indicating the inapplicability of the diffusion approximation in these cases.

D. Polarized Temporal Response

Temporal responses for multiple polarizations can be obtained from intensity frequency correlation data using the third-order correlation technique described in Subsection 2.D. With the 80 GHz frequency scanning range of our laser, we were able to effectively reconstruct the temporal responses for samples having a thicknesses of 12 mm and greater. These results for copolarized and cross-polarized light are given in Figs. 8–10 for the 12, 15, and 18 mm samples, respectively. A Hamming window was used to smooth the reconstructed temporal response, as described in Subsection 2.D. Because there is little difference between the LP and CP results for these samples, we do not make a distinction. The temporal responses for copolarized and cross-polarized light are clearly distinct for the 12- and 15-mm-thick samples, with the cross-polarized response being broader and less peaked. The result suggests that, on average, cross-polarized light is delayed relative to copolarized light. The temporal responses are in agreement with the second-order intensity correlation results of Fig. 7, which show that the copolarized light decorrelates slower with frequency than cross-polarized light. The temporal responses calculated from the diffusion model, assuming a reduced scattering coefficient of

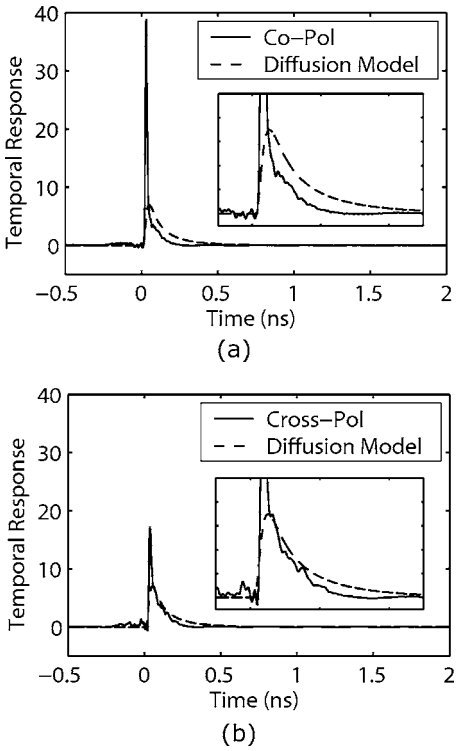

Fig. 8. Reconstructed temporal responses for the 12-mm-thick sample. The inset is a portion of the temporal responses enlarged for clarity. (a) Copolarized light (solid curve) compared with a diffusion model (dashed curve). (b) Cross-polarized light (solid curve) compared with a diffusion model (dashed curve).

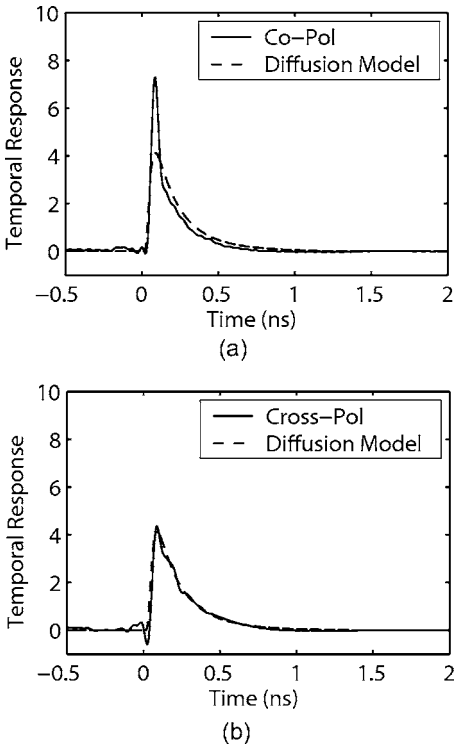

Fig. 9. Reconstructed temporal responses for the 15 mm sample. (a) Copolarized light (solid curve) compared with a diffusion model (dashed curve). (b) Cross-polarized light (solid curve) compared with a diffusion model (dashed curve).

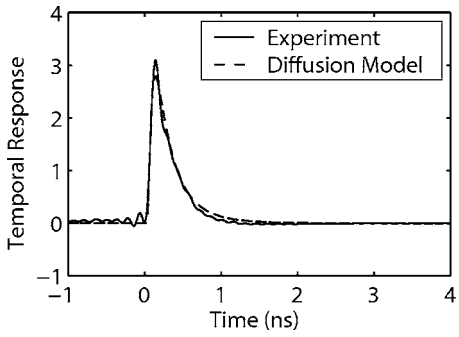

Fig. 10. Reconstructed temporal responses for the 18 mm sample (solid curve), regardless of polarization, compared with the diffusion model (dashed curve).

4 cm^{-1}, are presented as dashed curves in Figs. 8–10. Notice that the cross-polarized temporal response is predicted quite well, particularly for the 15 mm sample. This suggests that the cross-polarized light is more diffusive and contains less ballistic light and thus is more accurately approximated by the diffusion model. The 18 mm sample result in Fig. 10 has indistinguishable copolarized and cross-polarized temporal responses. The agreement between the measured data and the diffusion model is excellent. We can conclude that the diffusion model is only valid when the light is almost depolarized, as is the case for the cross-polarized light for the samples of moderate thickness.

5. SUMMARY

For scattering media where the fields are circular Gaussian, use of second- and third-order frequency correlations of speckle intensify patterns allows for the ensemble averaged impulse response to be determined to within an arbitrary time offset for multiple polarization states. The samples measured had scatterers whose size was small relative to the wavelength. Cross-polarized light was found to decorrelate faster with frequency than copolarized light and appears more diffusive. This is supported by the temporal response reconstructed using the third-order correlation technique. With less scatter, LP light was found to retain its polarization state better than CP, but in the transmission measurement, the CP cross-polarized light had a broader second-order frequency correlation. This difference diminishes with increasing scatter, as does the difference between copolarized and cross-polarized data. Comparison between the measured results and the diffusion approximation shows that this model is valid only in the regime where the light is almost depolarized.

ACKNOWLEDGMENT

This work was supported by the National Science Foundation under contracts 9901907-ECS, 0203240-ECS, and 0323037-ECS.

Corresponding author K. J. Webb can be reached by e-mail at webb@purdue.edu.

REFERENCES

1. S. R. Arridge, "Optical tomography in medical imaging," Inverse Probl. **15**, R41–R93 (1999).
2. A. B. Milstein, S. Oh, J. S. Reynolds, K. J. Webb, C. A. Bouman, and R. P. Millane, "Three-dimensional Bayesian optical diffusion tomography with experimental data," Opt. Lett. **27**, 95–97 (2002).
3. M. A. O'Leary, D. A. Boas, X. D. Li, B. Chance, and A. G. Yodh, "Fluorescence lifetime imaging in turbid media," Opt. Lett. **21**, 158–160 (1996).
4. A. B. Milstein, S. Oh, K. J. Webb, C. A. Bouman, Q. Zhang, D. A. Boas, and R. P. Millane, "Fluorescence optical diffusion tomography," Appl. Opt. **42**, 3081–3094 (2003).
5. A. B. Milstein, M. D. Kennedy, P. S. Low, C. A. Bouman, and K. J. Webb, "Detection and localization of a fluorescent mouse tumor in a turbid medium," Appl. Opt. **44**, 2300–2310 (2005).
6. J. D. McKinney, M. A. Webster, K. J. Webb, and A. M. Weiner, "Characterization and imaging in optically scattering media by use of laser speckle and a variable-coherence source," Opt. Lett. **25**, 4–6 (2000).
7. S. L. Jacques, J. R. Roman, and K. Lee, "Imaging superficial tissues with polarized light," Lasers Surg. Med. **26**, 119–129 (2000).
8. M. Moscosco, J. B. Keller, and G. Papanicolaou, "Depolarization and blurring of optical images by biological tissue," J. Opt. Soc. Am. A **18**, 948–960 (2001).
9. A. Ishimaru, "Diffusion of light in turbid material," Appl. Opt. **28**, 2210–2215 (1989).
10. K. Furutsu, "Diffusion equation derived from space-time transport equation," J. Opt. Soc. Am. **70**, 360–366 (1980).
11. C. A. Thompson, K. J. Webb, and A. M. Weiner, "Diffusive media characterization using laser speckle," Appl. Opt. **36**, 3726–3734 (1997).
12. D. Bicout, C. Brosseau, A. S. Martinez, and J. M. Schmitt, "Depolarization of multiply scattered waves by spherical diffusers: Influence of size parameter," Phys. Rev. E **49**, 1767–1770 (1994).
13. F. C. MacKintosh, J. X. Zhu, D. J. Pine, and D. A. Weitz, "Polarization memory of multiply scattered light," Phys. Rev. B **40**, 9342–9345 (1989).
14. I. Freund, "Optical intensity fluctuations in multiply scattering media," Opt. Commun. **81**, 251–258 (1991).
15. S. M. Cohen, D. Eliyahu, and M. Kaveh, "Vector statistics of multiply scattered waves in random systems," Phys. Rev. A **43**, 5748–5751 (1991).
16. I. I. Tarhan and G. H. Watson, "Polarization microstatistics of laser speckle," Phys. Rev. A **45**, 6013–6018 (1992).
17. P. Bruscaglioni, G. Zaccanti, and Q. Wei, "Transmission of a pulsed polarized light beam through thick, turbid media: numerical results," Appl. Opt. **32**, 6142–6150 (1993).
18. S. G. Demos and R. R. Alfano, "Optical polarization imaging," Appl. Opt. **36**, 150–155 (1997).
19. J. S. Tyo, M. P. Rowe, E. N. Pugh, Jr., and N. Engheta, "Target detection in optically scattering media by polarization-difference imaging," Appl. Opt. **35**, 1855–1870 (1996).
20. J. M. Schmitt, A. H. Gandjbakhche, and R. F. Bonner, "Use of polarized light to discriminate short path photons in a multiple scattering medium," Appl. Opt. **31**, 6535–6546 (1992).
21. S. P. Morgan, M. P. Khong, and M. G. Somekh, "Effects of polarization state and scatterer concentration on optical imaging through scattering media," Appl. Opt. **36**, 1560–1565 (1997).
22. A. H. Hielscher, J. R. Mourant, and I. J. Bigio, "Influence of particle size and concentration on the diffuse backscattering of polarized light from tissue phantoms and biological cell suspensions," Appl. Opt. **36**, 125–135 (1997).
23. A. Z. Genack, "Optical transmission in disordered media," Phys. Rev. Lett. **58**, 2043–2046 (1987).
24. L. G. Shirley and P. A. Lo, "Bispectral analysis of the wavelength dependence of speckle: remote sensing of object shape," J. Opt. Soc. Am. A **11**, 1025–1046 (1994).
25. M. A. Webster, K. J. Webb, A. M. Weiner, J. Y. Xu, and H. Cao, "Temporal response of a random medium from speckle intensity frequency correlations," J. Opt. Soc. Am. A **20**, 2057–2070 (2003).
26. M. A. Webster, T. D. Gerke, A. M. Weiner, and K. J. Webb, "Spectral and temporal speckle field measurements of a random medium," Opt. Lett. **29**, 1491–1493 (2004).
27. T. D. Gerke, M. A. Webster, A. M. Weiner, and K. J. Webb, "Frequency-resolved interferometer measurement of polarized wave propagation in scattering media," J. Opt. Soc. Am. A **22**, 2691–2699 (2005).
28. J. W. Goodman, *Statistical Optics* (Wiley, 1985).
29. I. S. Reed, "On a moment theorem for complex Gaussian processes," IRE Trans. Inf. Theory **8**, 194–195 (1962).
30. V. D. Hulst, *Light Scattering by Small Particles* (Wiley, 1957).
31. S. Chandrasekhar, *Radiative Transfer* (Oxford U. Press, 1960).
32. J. J. Duderstadt and L. J. Hamilton, *Nuclear Reactor Analysis* (Wiley, 1976).
33. M. Testorf, U. Osterberg, B. Pogue, and K. Paulsen, "Sampling of time- and frequency-domain signals in Monte Carlo simulations of photon migration," Appl. Opt. **38**, 236–245 (1999).
34. X. Wang, L. V. Wang, C. Sun, and C. Yang, "Polarized light propagation through scattering media: time-resolved Monte Carlo simulations and experiments," J. Biomed. Opt. **8**, 608–617 (2003).
35. M. Xu, "Electric field Monte Carlo simulation of polarized light propagation in turbid media," Opt. Express **12**, 6530–6539 (2004).
36. T. Aruga and T. Igarashi, "Narrow beam light transfer in small particles: image blurring and depolarization," Appl. Opt. **20**, 2698–2705 (1981).
37. M. S. Patterson, B. Chance, and B. C. Wilson, "Time resolved reflectance and transmittance for the non-invasive measurement of tissue optical properties," Appl. Opt. **28**, 2331–2336 (1989).
38. C. Brosseau, *Fundamentals of Polarized Light: a Statistical Optics Approach* (Wiley-Interscience, 1998).
39. A. Z. Genack and J. M. Drake, "Relationship between optical intensity, fluctuations and pulse propagation in random media," Europhys. Lett. **11**, 331–336 (1990).
40. M. A. Webster, K. J. Webb, and A. M. Weiner, "Temporal response of a random medium from third order laser speckle frequency correlations," Phys. Rev. Lett. **88**, 033901 (2002).
41. A. W. Lohmann and B. Wirnitzer, "Triple correlations," Proc. IEEE **72**, 889–901 (1984).
42. H. Bartelt, A. W. Lohmann, and B. Wirnitzer, "Phase and amplitude recovery from bispectra," Appl. Opt. **23**, 3121–3129 (1984).
43. S. Chandrasekhar, *Digital Signal Processing: Spectral Computation and Filter Design* (Oxford U. Press, 2001).
44. J. W. Goodman, *Introduction to Fourier Optics*, 2nd ed. (Wiley, 1996).
45. E. Kogan and M. Kaveh, "Statistics of fluctuations for two types of crossover: From the ballistic to diffusive regime and from the orthogonal to unitary ensemble," Phys. Rev. B **51**, 16400–16402 (1995).
46. A. A. Chabanov and A. Z. Genack, "Field distributions in the crossover from ballistic to diffusive wave propagation," Phys. Rev. E **56**, R1338–R1341 (1997).
47. A. Garcia-Martin, J. J. Saenz, and M. Nieto-Vesperinas, "Spatial field distributions in the transition from ballistic to diffusive transport in randomly corrugated waveguides," Phys. Rev. Lett. **84**, 3578–3581 (2000).
48. A. Ishimaru, S. Jaruwatanadilok, and Y. Kuga. "Polarized pulse waves in random discrete scatterers," Appl. Opt. **40**, 5495–5502 (2001).